Publ. Astron. Soc. Japan (2014) 00(0), 1–14
doi: 10.1093/pasj/xxx000

THE SUBARU COSMOS 20: SUBARU OPTICAL IMAGING OF THE HST COSMOS FIELD WITH 20 FILTERS*

Y. TANIGUCHI[1], M. KAJISAWA[1, 2], M. A. R. KOBAYASHI[1], Y. SHIOYA[1], T. NAGAO[1], P. CAPAK[3], H. AUSSEL[4], A. ICHIKAWA[1, 2], T. MURAYAMA[5], N. SCOVILLE[3], O. ILBERT[6], M. SALVATO[7], D. B. SANDERS[8], B. MOBASHER[9], S. MIYAZAKI[10], Y. KOMIYAMA[10], O. LE FÈVRE[6], L. TASCA[6], S. LILLY[11], M. CAROLLO[11], A. RENZINI[12], M. RICH[13], E. SCHINNERER[14], N. KAIFU[15], H. KAROJI[16], N. ARIMOTO[17], S. OKAMURA[18], K. OHTA[19], K. SHIMASAKU[20] and T. HAYASHINO[21]

*Based on data collected at Subaru Telescope, which is operated by the National Astronomical Observatory of Japan.

[1]Research Center for Space and Cosmic Evolution, Ehime University, 2-5 Bunkyo-cho, Matsuyama 790-8577, Japan
[2]Physics Department, Graduate School of Science & Engineering, Ehime University, 2-5 Bunkyo-cho, Matsuyama 790-8577, Japan
[3]California Institute of Technology, MC 105-24, 1200 East California Boulevard, Pasadena, CA 91125, USA
[4]AIM Unité Mixte de Recherche CEA CNRS, Université Paris VII UMR n158, F-75014 Paris, France
[5]Astronomical Institute, Graduate School of Science, Tohoku University, Aramaki, Aoba, Sendai 980-8578, Japan
[6]Aix Marseille Université , CNRS, LAM (Laboratoire d'Astrophysique de Marseille), UMR 7326, 13388, Marseille, France
[7]Max Planck Institut für Plasma Physik and Excellence Cluster, 85748 Garching, Germany
[8]Institute for Astronomy, 2680 Woodlawn Drive, University of Hawaii, Honolulu, HI, 96822, USA
[9]Department of Physics and Astronomy, University of California, Riverside, CA 92521, USA
[10]National Astronomical Observatory of Japan, 2-21-1 Osawa, Mitaka, Tokyo 181-8588, Japan
[11]Institute for Astronomy, Department of Physics, ETH Zurich, CH-8093 Zurich, Switzerland
[12]INAF - Osservatorio Astronomico di Padova, vicolo dell'Osservatorio 5, 35122, Padova, Italy
[13]Department of Physics and Astronomy, University of California, Los Angeles, CA 90095, USA
[14]Max Planck Institut für Astronomie, Königstuhl 17, Heidelberg, D-69117, Germany
[15]The Open University, 2-11, Wakaba, Mihama-ku. Chiba 261-8586, Japan
[16]Kavli Institute for the Physics and Mathematics of the Universe (Kavli IPMU, WPI), The University of Tokyo, Chiba 277-8582, Japan
[17]Subaru Telescope, 650 N. A'ohoku Place, Hilo, HI 96720, USA
[18]Department of Advanced Sciences, Faculty of Science and Engineering, Hosei University, 3-7-2 Kajino-cho, Koganei-shi, Tokyo 184-8584, Japan
[19]Department of Astronomy, Graduate School of Science, Kyoto University, Kitashirakawa, Sakyo-ku, Kyoto 606-8502, Japan

[20]Department of Astronomy, Graduate School of Science, The University of Tokyo, 7-3-1 Hongo, Bunkyo-ku, Tokyo 113-0033, Japan
[21]Research Center for Neutrino Science, Tohoku University, Aramaki-Aza-Aoba, Aoba-ku, Sendai 980-8588, Japan

Received 2015 January 30; Accepted 2015 October 2

Abstract

We present both the observations and the data reduction procedures of the Subaru COSMOS 20 project that is an optical imaging survey of the *HST* COSMOS field, carried out by using Suprime-Cam on the Subaru Telescope with the following 20 optical filters: 6 broad-band (B, g', V, r', i', and z'), 2 narrow-band (NB711 and NB816), and 12 intermediate-band filters (IA427, IA464, IA484, IA505, IA527, IA574, IA624, IA679, IA709, IA738, IA767, and IA827[1]). A part of this project is described in Taniguchi et al. (2007) and Capak et al. (2007) for the six broad-band and one narrow-band (NB816) filter data. In this paper, we present details of the observations and data reduction for remaining 13 filters (the 12 IA filters and NB711). In particular, we describe the accuracy of both photometry and astrometry in all the filter bands. We also present optical properties of the Suprime-Cam IA filter system in Appendix.

Key words: methods: observational — surveys — techniques: photometric

1 INTRODUCTION

The Cosmic Evolution Survey (COSMOS) is a treasury program on the *Hubble Space Telescope* (*HST*), awarded a total of 590 *HST* orbits, carried out in Cycles 12 and 13 (Scoville et al. 2007a, 2007b; Koekemoer et al. 2007). In total, a sky area of 1.64 square degree is covered with Advanced Camera for Surveys (ACS) F814W filter around the central position $\mathrm{R.A.(J2000)} = 10^h\ 00^m\ 28.6^s$ and $\mathrm{Decl.(J2000)} = +02^\circ\ 12'\ 21.0''$. Note that we originally proposed to map a $1.4\ \mathrm{degree} \times 1.4\ \mathrm{degree} = 2$ square degree field. However, due to the observational constraints, the sky area of 1.64 square degree was mapped (Koekemoer et al. 2007). On the other hand, the Subaru COSMOS 20 project has covered the whole 2 square degree field. The comparison between the *HST* ACS field and the Subaru COSMOS 20 field is shown in Figure 1. A point source limiting magnitude is down to $\mathrm{AB(F814W)} = 27.2$ (5σ, $0.''24$ diameter aperture). These ACS observations provide us a large sample of galaxies with a spatial resolution of 0.1 arcsec covering a redshift range between $z \sim 0$ to $z \sim 6$ (e.g., Taniguchi et al. 2009; Murata et al. 2014; Kobayashi et al. 2015).

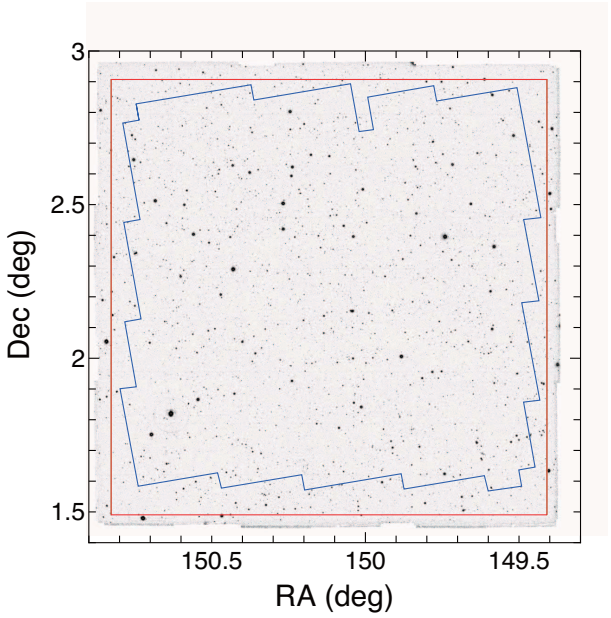

Fig. 1. The whole COSMOS field of $1.95\ \mathrm{deg}^2$ (red line) and the ACS field of $1.64\ \mathrm{deg}^2$ (blue line) overlaid on the IA427 band image.

The main purpose of the COSMOS project is to understand the evolution of galaxies, active galactic nuclei (or super massive black holes), and dark matter halos together with the evolution of large scale structures in the Universe. In order to carry out this project, we also need multi-wavelength data from X-ray, ultraviolet though optical to infrared and radio. Indeed, such multi-wavelength campaign has been made intensively: X-ray (Hasinger et al. 2007; Elvis et al. 2009), ultraviolet (Zamojski et al. 2007), optical (Taniguchi et al. 2007; Capak et al. 2007), infrared (Sanders et al. 2007), and radio (Schinnerer et al. 2007; Smolčić et al. 2012). Among them, optical imaging observations made by use of Suprime-Cam (Miyazaki et al. 2002) on the Subaru Telescope (Kaifu et al. 2000; Iye et al. 2004) are highly useful to investigate both photometric properties and photometric redshifts of the galaxies found in the COSMOS field (Mobasher et al. 2007; Ilbert et al. 2009; Salvato et al. 2009).

In our Subaru COSMOS 20 project, we used 20 filters in the optical covering from 400 nm to 900 nm: six broad-band (B, g', V, r', i', and z'), twelve intermediate-band (IA427, IA464, IA484, IA505, IA527, IA574, IA624, IA679, IA709, IA738, IA767, and IA827), and two narrow-band filters (NB711 and NB816). This is the origin of the project's name, "Subaru COSMOS 20". Since we have already given a detailed description on the broad-band and NB816 imaging of the COSMOS field (Taniguchi et al. 2007; hereafter Paper I), we present details of observations, data reductions, calibration, and quality assessment for the twelve intermediate-band filters and NB711 in this paper (see also Capak et al. 2007). As for the NB711 imaging of the COSMOS field, see also Shioya et al. (2009) and Kajisawa et al. (2013). In Appendix, we present a summary of the optical properties of the Suprime-Cam IA filter system. Throughout this paper, we use the AB magnitude system.

The twelve intermediate-band filters are selected from the Suprime-Cam IA filter set (Hayashino et al. 2000; Taniguchi et al. 2004). The spectral resolution of all the IA filters is $R = \lambda/\Delta\lambda \approx 23$, being just intermediate between typical broad-band filters ($\lambda/\Delta\lambda \sim 5$) and narrow-band filters ($\lambda/\Delta\lambda \sim 50$–100). Therefore, imaging with multi-IA filters is equivalent to low-resolution spectroscopy with an $R \approx 23$ (see, for example, Yamada et al. 2005). It is also mentioned that the use of IA filters makes it possible to detect very strong emission-line objects (galaxies or active galactic nuclei). Although such objects tend to be rare, some examples have been discovered to date: ultra strong emission line galaxies (USELs) defined as $\mathrm{EW(H}\beta) \geq 30$ Å (Kakazu et al. 2007), and Green Pea objects found in the Galaxy Zoo project (Cardamone et al. 2009).

Since such very strong emission lines in galaxies affect broad-band colors of the galaxies (e.g., Nagao et al. 2007), careful analyses are recommended to make any sample selection of a particular class of galaxies. For example, in the case of color selection of very high redshift galaxies at $z \sim 7$–8, strong emission line galaxies at $z \sim 2$ with little stellar continuum can act as interlopers (see Taniguchi et al. 2010; Atek et al. 2011). On the other hand, such very strong emission line galaxies themselves are important populations, because most of them are very metal poor galaxies (Kakazu et al. 2007; Amorín et al. 2014, 2015). Therefore, surveys of such objects contribute to the understanding chemical evolution of galaxies.

In our Subaru COSMOS 20 project, we also use the two narrow-band filters, NB711 and NB816. Imaging with such narrow-band filters provides us samples of targeted emission line galaxies. For example, NB816 has been used to find Lyα emitters at $z = 5.7$ (e.g., Hu et al. 2004, 2010; Shimasaku et al. 2005; Murayama et al. 2007). However, the use of NB816 also provides us samples of Hα emitters at $z = 0.24$ (Shioya et al. 2008) and [O II] emitters at $z = 1.2$ (Takahashi et al. 2007; Ideue et al. 2009, 2012). In the case of COSMOS project, NB711 has also been used to sample both Lyα emitters at $z = 4.9$ (Shioya et al. 2009) and [O II] emitters at $z = 0.9$ (Kajisawa et al. 2013). Therefore, if we combine imaging surveys with multiple NB filters, we can trace the cosmic star formation history from high to low redshifts (e.g., Hopkins 2004; Shioya et al. 2008).

Moreover, multi-band optical imaging such as our Subaru COSMOS 20 improves the accuracy of photometric redshifts of galaxies (Ilbert et al. 2009) and active galactic nuclei (Salvato et al. 2009, 2011). The accurate photometric redshifts for the large sample of galaxies allow us to map the large-scale structure at various redshifts and to study the environmental effects of the galaxy evolution (Feruglio et al. 2010; Scoville et al. 2013). One can also combine such photometric redshifts with a smaller spectroscopic sample to estimate the overdensity of galaxies with high accuracy (e.g., Kovač et al. 2014) and to measure the clustering strength of AGNs (Georgakakis et al. 2014).

2 OBSERVATIONS

2.1 Observational Strategy

The COSMOS field covers an area of $1.^{\circ}4 \times 1.^{\circ}4$, centered at $\mathrm{R.A.} = 10^{\mathrm{h}}\ 00^{\mathrm{m}}\ 28.6^{\mathrm{s}}$ and $\mathrm{Decl.} = +02^{\circ}\ 12'\ 21.0''$. The Suprime-Cam consists of ten 2048×4096 CCD chips and provides a very wide field of view, $34' \times 27'$ in 10240×8192 pixels ($0.''202$ pixel^{-1}) (Miyazaki et al. 2002). Although the field of view of the Suprime-Cam had been the widest one among available imagers on the 8–10 m class telescopes before Hyper Suprime Cam on the Subaru Telescope (Miyazaki et al. 2012), we needed multiple pointings to cover the entire COSMOS field.

In our previous Suprime-Cam observations, we used the two dithering patterns, Pattern A and Pattern C (Paper I). Pattern A consists of $12\ \mathrm{shots} \times 4$ sets (48 shots in total) to cover the whole COSMOS field (see Figure 1 in Paper I). This dithering pattern is a half-array shifted mapping method to obtain accurate astrometry and a self-consistent photometric solution across the entire field. Another dithering method is Pattern C that consists of $9\ \mathrm{shots} \times 4$ sets (36 shots in total) to cover the whole COSMOS field efficiently (see Figure 2 in Paper I). It is noted that both patterns are designed to take care of spatial gaps ($3''$–$4''$ or $16''$–$17''$) between the CCD chips of the Suprime-Cam.

After our previous observations, we confirmed that observations with Pattern C only are enough to obtain accurate photometry and astrometry. The flat frames generated using only Pattern C in the broad bands are consistent with those created with both Pattern A and Pattern C within 1% root mean square. Therefore, our new observations with the intermediate and narrow-band filters were made by using Pattern C. This made our observations more efficient than our previous obser-

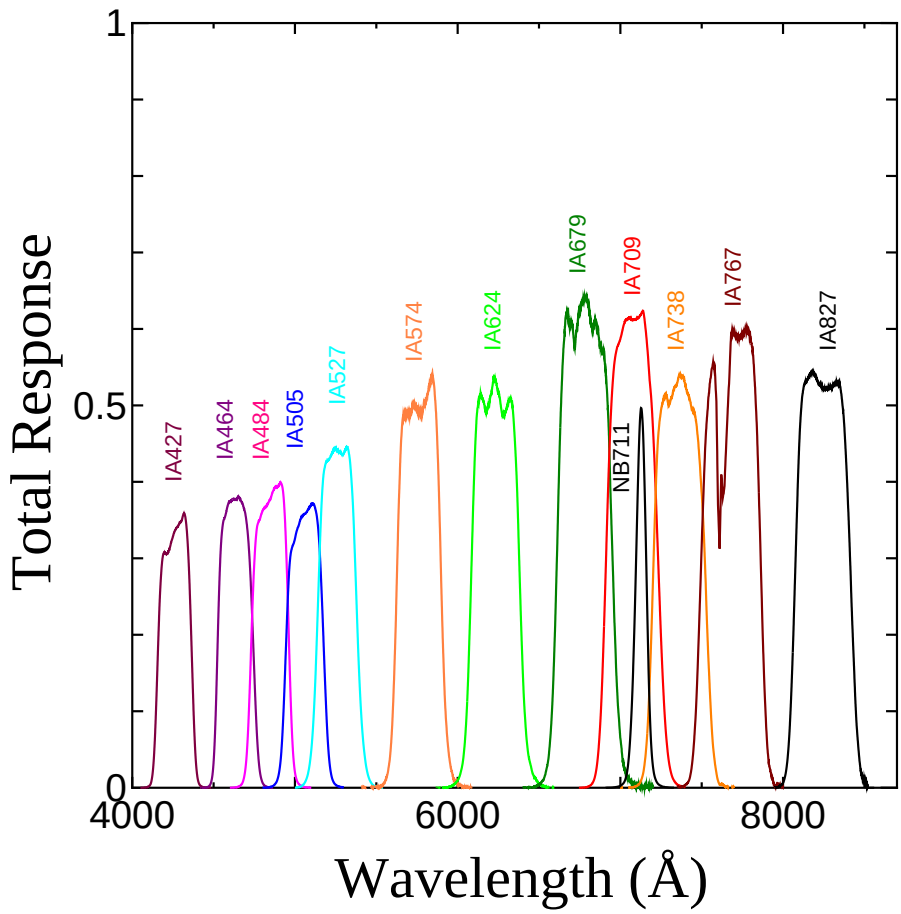

Fig. 2. Filter response curves at the center of the filter, including effects of the CCD sensitivity, the atmospheric transmission, and the transmission of the telescope and the instrument.

vations.

In this paper, we used twelve intermediate-band filters (IA427, IA464, IA484, IA505, IA527, IA574, IA624, IA679, IA709, IA738, IA767, and IA827) and one narrow-band filter (NB711). Note that we intended to use another NB filter, NB921, whose effective wavelength and the full width at half maximum (FWHM) are $\lambda_{\rm eff} = 9196$ Å and $\Delta\lambda = 132$ Å, respectively (Kodaira et al. 2003; Kashikawa et al. 2004; Taniguchi et al. 2005). However, we did not have enough time to take any NB921 data.

The filter response curves including the CCD sensitivity and the atmospheric transmission are shown in Figure 2 for the twelve IA filters and NB711 (see also Section 3.2 for details). In Figure 3, we also show those for the 20 filters used in Subaru COSMOS 20. In order to see the wavelength coverage fairly, all the response curves are normalized; i.e., all the peak values are set to be unity. Note that the current CCD chips[1] installed on Suprime-Cam are different from those used in our Subaru COSMOS 20 project.

[1] These new CCD chips were installed on July 2008; see for details the following URL, http://www.naoj.org/Observing/Instruments/SCam/parameters_mit.html.

2.2 Observational Programs and Runs

Our Suprime-Cam observations of the COSMOS field have been made during a period between 2006 January and 2007 March, consisting of two open-use observing programs: S05B-013I (COSMOS-21: Deep Intermediate & Narrow-band Survey of the COSMOS Field) and S06B-026 (COSMOS-21: Deep Intermediate-band Survey of the COSMOS Field). The first one is an Intensive Program on the Subaru Telescope. Fourteen and half nights were allocated for these two proposals (Tables 1 and 2). With 28.5 nights (including 4 compensation nights) allocated for our COSMOS observations in Paper I, 43 nights were allocated in total.

Our observations in the available nights shown in Table 2 were made under the photometric conditions except for the IA505- and IA679-bands observations on Feb. 24, 2006. We observed the spectrophotometric standard stars immediately before and after the target observations for the photometric calibration. These standard stars have been observed at various

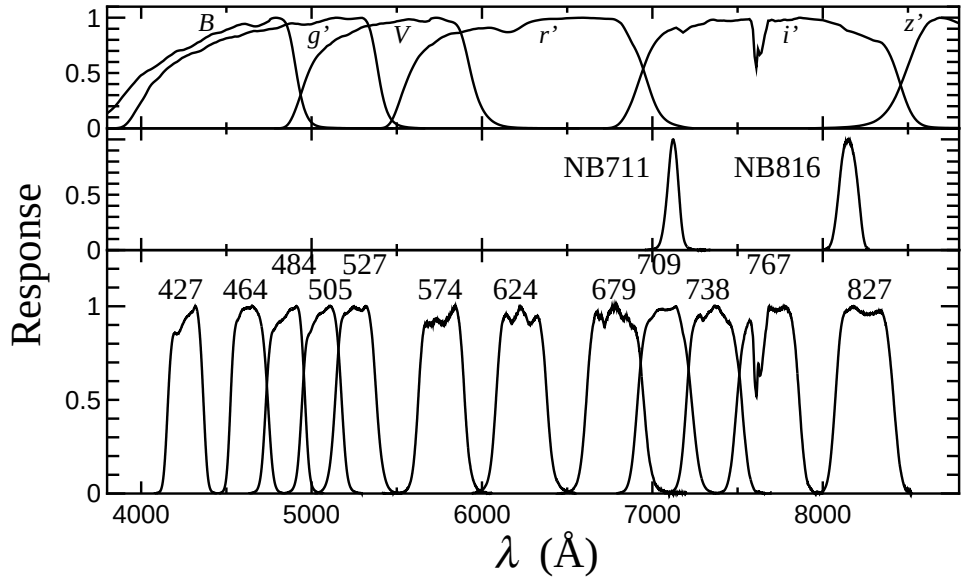

Fig. 3. Filter response curves at the center of the broad-band filters (upper panel), narrow-band filters (middle panel), and intermediate-band filters (lower panel) used in the Subaru COSMOS 20 project. These response curves include the CCD sensitivity, the atmospheric transmission, and the transmission of the telescope, the instrument, and the filter. These curves are normalized to a maximum response of 1.

Table 1. A summary of observational programs.

Semester	ID No.[a]	PI	Program Title	Nights	Paper[b]
S03B	239I	Y. Taniguchi	COSMOS-Broad[c]	10	1
S04A	080	Y. Taniguchi	COSMOS-Narrow[d]	2.5	1
S04B	142I	Y. Taniguchi	COSMOS-21[e]	8	1
S04B	UH-17A	N. Scoville	COSMOS-21[e]	4	1
S05B	013I	Y. Taniguchi	COSMOS-21[e]	10	2
S06B	026	Y. Taniguchi	COSMOS-21[f]	4.5	2

[a] The figure "I" given in the last of ID number means an Intensive Program.
[b] $1 = \mathrm{Paper\ I}$, and $2 = \mathrm{this\ paper}$.
[c] Suprime-Cam Imaging of the *HST* COSMOS 2-Degree ACS Survey Deep Field (Intensive Program).
[d] Wide-Field Search for Lyα Emitters at $z = 5.7$ in the *HST*/COSMOS Field.
[e] COSMOS-21: Deep Intermediate & Narrow-band Survey of the COSMOS Field (Intensive Program).
[f] COSMOS-21: Deep Intermediate-band Survey of the COSMOS Field.

airmass, defocussing the telescope to avoid saturation. The observed standard stars are summarized in Table 3. Although we also observed GD 71 with several IA filters, all the data were saturated and we did not use GD 71 for the photometric calibration.

3 DATA REDUCTION AND IMAGE QUALITY

3.1 Data Reduction

All the individual CCD data were reduced using IMCAT[2] with the same manner as the Suprime-Cam broad-band data of the COSMOS survey (Capak et al. 2007). At first, we performed the bias subtraction and the masking of bad or saturated pixels. Then the flat fielding was carried out with the median dome flats. We subtracted the median sky frames from the flat-fielded object frames to remove the night sky illumination and fringe pattern. The residual background was measured in a grid of 128×128 pixel squares after masking objects and subtracted.

After the sky subtraction, we calculated an astrometric solution for each CCD chip in all frames using the COSMOS astrometric reference catalog. This catalog was build in 2004 using the Megacam i^*-band data (Capak et al. 2007), a dataset with bright enough saturation magnitude on individual exposures ($i^* = 16$) to be registered on classical astrometric references, and deep enough (reaching $i^* = 24$) to allow for the registration of all other Subaru and ACS COSMOS data. The COSMOS astrometric reference catalog was build iteratively via the following four steps: 1) the astrometric solution for the Megacam images was computed using the Astrometrix soft-

[2] IMCAT is distributed by Nick Keiser at http://www.ifa.hawaii.edu/~kaiser/imcat/

Table 2. A summary of observational runs.

ID No.[a]	Period	Nights	Avail. Nights	Bands	Paper[b]
S03B-239I	2004 Jan 16–21	6	5	B, r', i', z'	1
S03B-239I	2004 Feb 15–18	4	2	V, i'	1
S04A-080	2004 Apr 15–19[c]	2.5	1	$NB816$	1
S04B-142I	2005 Jan 8–10	3	0	no data	1
UH-17A	2005 Feb 3	1	0	no data	1
S04B-142I	2005 Feb 9–13	5	2	g', V, $NB816$	1
UH-17A	2005 Mar 10–12	3	1	$NB816$	1
S04B-142I	2005 Apr 1–4[d]	4	3	g', $NB816$	1
S05B-013I	2006 Jan 27–Feb 1[e]	6	6	$IA427$, $IA574$, $IA709$, $IA827$, $NB711$	2
S05B-013I	2006 Feb 22–25	4	3	$IA464$, $IA505$, $IA679$	2
S06B-026	2006 Dec 17–19[f]	1.5	1.5	$IA624$, $IA679$	2
S06B-026	2007 Jan 15–18[f]	2	2	$IA484$, $IA527$, $IA738$	2
S06B-026	2007 Mar 20–22[e, g]	1	1	$IA767$	2

[a] The figure "I" given in the last of ID number means an Intensive Program.

[b] $1 = \mathrm{Paper\ I}$, and $2 = \mathrm{this\ paper}$.

[c] First half night was used in every night.

[d] Compensation nights because of the poor weather in S04B-142 Jan and Feb runs.

[e] Observing time exchange with Dave Jewitt (IfA, UH).

[f] Second half night was used in every night.

[g] Three hours $\times$ 3.

Table 3. A summary of standard stars.

Band	Standard stars
B	SA 95-193, SA 98-685, SA 101-207, SA 104
V	SA 95-193, SA 101-207, SA 104
g'	G 163-51, SA 101-207
r'	Feige 22, Rubin 149F, SA 95-193, SA 98-685, SA 101-207
i'	Feige 22, Rubin 149F, Rubin 152, SA 95-193, SA 98-685, SA 101-207
z'	Feige 22, Rubin 152, SA 95-193, SA 98-685, SA 101-207
$IA427$	GD 50, GD 108, HZ 4, HZ 21, HZ 44
$IA464$	GD 50, GD 108, HZ 4
$IA484$	GD 50, GD 108, HZ 4, HZ 21, HZ 44
$IA505$	GD 50, GD 108, HZ 4, HZ 21, HZ 44
$IA527$	GD 50, GD 108, HZ 4, HZ 21
$IA574$	GD 50, GD 108, HZ 4, HZ 21, HZ 44
$IA624$	GD 50, GD 108, HZ 4, HZ 21, HZ 44
$IA679$	GD 108, HZ 21, HZ 44
$IA709$	GD 50, GD 108, HZ 4, HZ 21, HZ 44
$IA738$	GD 50, GD 108, HZ 4, HZ 21
$IA767$	GD 50, GD 108, HZ 4, HZ 21, HZ 44
$IA827$	GD 50, GD 108, HZ 4, HZ 21, HZ 44
$NB711$	GD 50, GD 108, HZ 4, HZ 21, HZ 44
$NB816$	Feige 34, GD 50, GD 108, HZ 4

ware (Radovich et al. 2001), that was at the time part of the Terapix pipeline (SCAMP was only introduced in 2005), using the USNO-B1.0 catalog (Monet et al. 2003) as reference. 2) The i^*-band catalog obtained from the Megacam stack was cross-matched to the COSMOS VLA pre survey (Schinnerer et al. 2004), and we measured offsets of $\Delta\alpha\cos\delta = 16.1 \pm 4.1$ mas and $\Delta\delta = -144.0 \pm 4.0$ mas, without any indication of variation across the field. 3) The measured offsets were applied to the input USNO-B1.0 catalog, and the astrometric solution of the Megacam i^*-band images was recomputed in the same manner as step 1. 4) The final COSMOS astrometric reference catalog was obtained from the i^*-band Megacam stack produced at step 3. The internal accuracy of the COSMOS astrometric reference, i.e., the maximum value of the residual of the astrometric solution derived by Astrometrix when fitting the shifted USNO-B1.0 catalog is $\Delta\alpha\cos\delta = -26.8 \pm 4.0$ mas and $\Delta\delta = -18.6 \pm 4.9$ mas, and the absolute offset to the full survey VLA astrometry is $\Delta\alpha\cos\delta = -55.8 \pm 3.8$ mas and $\Delta\delta = 81.4 \pm 4.2$ mas. All our COSMOS 20 images were forced to the COSMOS astrometric reference using a 3–5th order polynomial. The polynomial order was increased until the astrometric errors were consistent with the seeing size in the data. The internal scatter of the resulting astrometry is always less than 0.2 arcsec.

We then performed the scattered light correction for the flat as described in Capak et al. (2007). The dome and sky flat can be affected by the scattered light at 3–5% level. The correction factor for this effect was calculated in each 128×128 pixel grid so that the background subtracted fluxes of an object at different positions of the detector in the different frames have the same values. Objects in the all frames were simultaneously used in the fitting procedure for each band. In this process, we also added the additional correction factor for each frame to take account of the effects of the airmass and non-photometric condition. These correction factors for the scattered light in each region and for the atmospheric condition in each frame were simultaneously determined in the fitting for each band (equations (1) and (2) in Capak et al. 2007). Thus we made the corrected flat frames and applied them to the object frames.

Then the frame to frame offsets of the background-subtracted fluxes of objects were examined as a function of airmass and Modified Julian Date. If the data followed the airmass trend estimated from the standard star observations within the expected 1–2% error due to point spread function (PSF) variation, the data were deemed photometric. If data stopped following the expected trend, or did not follow it for a night, the data were deemed non photometric. The non-photometric frames were scaled to the mean of the airmass corrected photometric data. The frames with extinction greater than 0.5 mag were discarded. In the case of the IA679 band, where no photometric data were obtained, all the object frames were scaled to the least extinct frame. Therefore the photometry in the IA679 band should be used with caution.

The flux-matched frames were then smoothed to the same PSF FWHM using a Gaussian kernel. After the resampling onto the final astrometric grid, the PSF-matched frames were combined with a weight of the inverse variance of each frame, clipping outlier values at more than 5σ from the median value in the calculation of each pixel. In this procedure, we also generated a root mean square (rms) map that reflects the true pixel-to-pixel rms, which is the value expected if the effects of the resampling and smoothing do not exist. The rms measured in a given area on this rms map represents the variance that would be measured in the background of the same area if the variance was calculated on the individual images that went into the final mosaiced image. The PSF sizes of final images are summarized in Table 4. In addition to these PSF-matched combined images, we also provided the original-PSF images for each band from the frames that were not convolved in order to provide a maximum sensitivity for detection of (compact) sources. Note that the PSF varies as a function of position in these original-PSF images, and therefore the color measurements with a relatively small aperture can be less reliable. These reduced images were divided into tiles with a dimension of $10' \times 10'$ as shown in Figure 5 of Paper I.

For the color measurements and generating the official multi-band photometric catalog, we additionally convolved the PSF-matched combined images to match the PSF among all the optical–NIR data from U to $K_{\rm s}$ band. These data were convolved with a Gaussian kernel so that the flux ratio between a $3''$ and $10''$ aperture for a point source in each band is the same as that of CTIO/KPNO $K_{\rm s}$-band data, which have the lowest flux ratio of ~ 0.75 (Capak et al. 2007). The width (σ-value) of the Gaussian kernel used in the convolution of the IA and $NB711$-band data is shown in the last column of Table 4. Using these convolved data, we carried out the multi-band photometry with a $3''$ diameter aperture and the results are presented in the official photometric catalog. Note that the matching of the flux ratio between $3''$ and $10''$ apertures for point sources does not necessarily guarantee the same flux ratio for extended sources, because the detailed shapes of the PSF are not the same among the different bands. If one needs to measure colors for extended sources with high accuracy, the photometric values in the official catalog should be used with caution.

3.2 Photometric Calibration

Since we used the original intermediate- and narrow-band filters in this project, the theoretical synthetic magnitudes of the spectrophotometric standard stars are necessary for the photometric calibration. The theoretical complete system response in each band was computed by multiplying the filter transmis-

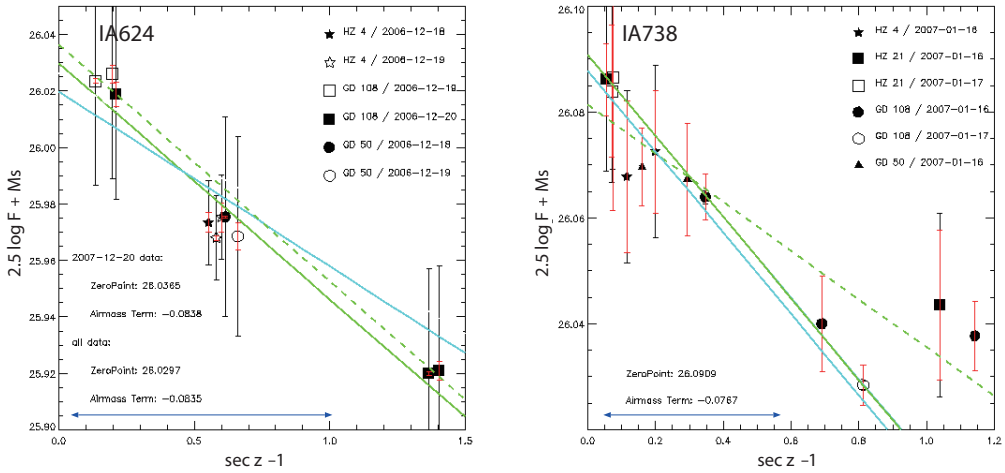

Fig. 4. Determination of the photometric zero points for the IA624 (left) and IA738 (right) bands. Each symbol represents a different standard star and a different night of observation. The red error bars correspond to the uncertainty of the theoretical magnitudes (see Table B1) and the black ones represent the combined counts measurements and uncertainty of the standard. The airmass relation obtained from the object frames of the survey is given by the cyan line. The green dashed line is a fit to all data of the standard stars, while the solid green line is a fit excluding nights where there was indication that the standard measurements were not obtained under photometric conditions (i.e., the data represented as the filled symbols). The agreement between the two airmass determination is reasonable for IA624, and good for IA738 for the standard data obtained on 2007-01-17 (the open symbols), while quite poor for the standard data obtained in 2007-01-16 (the filled symbols). The range of $(\sec z - 1)$ for the targets is shown by the blue horizontal arrow in each panel.

sion, the Subaru telescope mirror reflectivity, the prime focus unit's transmission, the CCD quantum efficiency, and the atmosphere transmission for an airmass of 1.2. For the atmosphere, we used the same model as the one used for the broad-band Suprime-Cam filters (K. Shimasaku, private communication[3]). We computed the theoretical synthetic magnitude in the AB system of our standard stars using the available `CALSPEC`[4] spectra, i.e., `gd50_004.fits` for GD 50, `gd108_005.fits` for GD 108, `hz4_stis_001.fits` for HZ 4, `hz21_stis_001.fits` for HZ 21 and `hz44_stis_001.fits` for HZ 44 (Bohlin 1996; Bohlin et al. 2001). We present these theoretical magnitudes in the Appendix B. Note that for the HZ stars, the `CALSPEC` spectra have been interpolated between 5150 Å and 5212 Å, resulting in a larger overall uncertainty in the calibration of the IA505 and IA527 bands, because this more uncertain region lies on the edges of these two passbands.

These standard stars have been observed at various airmass as mentioned above, and we determined the zero point for each band taking account of the airmass dependence. If F are the counts measured from the standard star under an airmass $\sec z$, the relation between the standard magnitude $M_{\rm s}$ and the zero point $Z_{\rm p}$ is:

$$-2.5\log F + Z_{\rm p} - M_{\rm s} = k(\sec z - 1) \quad (1)$$

So that the airmass term k is the slope of the expected linear fit to the data of the standard stars and its intercept gives the zero point. Figure 4 shows typical examples of the calibration for the IA624 and the IA738 bands. For most bands, our zero point determination is accurate within 0.02 mag. In a few cases, there was a lack of standard star observations at high airmass that prevented us to derive the airmass term from the standard star data. In this case, we used the airmass point of the object data for the zero-point determination. Note that for the IA679 band, we obtained no photometric data both for the COSMOS field and the standard stars, and we scaled to the photometry of the neighboring bands (i.e., IA624 and IA709) assuming the objects were flat in F_ν for the interpolation. After the photometric calibration, all the reduced images are converted to be in units of nanojanskys per pixel (the zero point of 31.4 mag in the AB magnitude system).

We also checked the consistency among the zero points in the different bands through the spectral energy distribution fitting for a large number of galaxies with spectroscopic redshift (Ilbert et al. 2009). The multi-band photometry from UV to MIR wavelength including the IA- and narrow-band data were fitted with population synthesis models, and the systematic difference between the model and observed magnitudes in a certain band is considered to reflect the zero-point offset. The details of the method to determine the zero-point offsets are described in Ilbert et al. (2006, 2009). These offsets of the photometric zero points are shown in the second-last column of Table 4. We note that the offset for the IA679 band is much higher than the other IA bands, which probably reflect the larger uncertainty in the photometric calibration for this band mentioned above. The zero-point offsets in Table 4 are calculated for the upgraded version (v2.0) of the photometric redshift cata-

[3] http://hikari.astron.s.u-tokyo.ac.jp/work/suprime/filters/
[4] See http://www.stsci.edu/hst/observatory/crds/calspec.html.

Table 4. A summary of the optical imaging data for COSMOS.

Band	$\lambda_{\rm eff}^{a}$ (Å)	FWHM^{b} (Å)	TDT^{c} (min)	$m_{\rm lim}^{d}$ (mag)	$\sigma_{m_{\rm lim}}^{e}$ (mag)	PSF FWHM^{f} ($''$)	offset^{g} (mag)	$\sigma_{\rm conv}^{h}$ ($''$)
$IA427$	4263.5	207.3	41.3	25.8	0.12	1.64	0.042	0.30
$IA464$	4635.1	218.1	40.0	25.6	0.13	1.89	0.040	0.29
$IA484$	4849.2	229.1	36.7	25.9	0.16	1.14	0.014	0.59
$IA505$	5062.5	231.5	36.0	25.6	0.13	1.44	0.013	0.48
$IA527$	5261.1	242.7	36.7	25.7	0.12	1.60	0.041	0.41
$IA574$	5764.8	272.8	45.3	25.4	0.10	1.71	0.085	0.11
$IA624$	6232.9	299.9	36.7	25.7	0.16	1.05	0.009	0.66
$IA679$	6781.1	335.9	41.3	25.3	0.10	1.58	-0.176	0.31
$IA709$	7073.6	316.3	40.0	25.4	0.10	1.58	-0.021	0.14
$IA738$	7361.5	323.8	37.0	25.4	0.10	1.08	0.021	0.59
$IA767$	7684.9	365.0	45.0	25.1	0.13	1.65	0.039	0.20
$IA827$	8244.5	342.8	72.0	25.1	0.15	1.74	-0.013	0.13
$NB711$	7121.7	72.5	35.0	25.0	0.13	0.79	0.014	0.72

[a] Effective wavelength calculated from the filter response curve including the effects of the CCD sensitivity, the atmospheric transmission, and the transmission of the telescope and the instrument shown in Figure 2.
[b] FWHM of the filter response curve mentioned above.
[c] The target dedicated time.
[d] The average 3σ limiting magnitude in the AB system within $3''$ diameter aperture.
[e] The standard deviation of $m_{\rm lim}$ measured in the 81 tiles.
[f] The PSF size of the final images. Note that the PSF of each filter band is finally matched so that the flux ratio between a $3''$ and $10''$ apertures is the same as that in the CTIO/KPNO $K_{\rm s}$-band data to provide official photometric catalog (see text).
[g] Systematic offset of the photometric zero point for each filter (see text).
[h] The σ-value of the Gaussian kernel used for the PSF matching among the different bands (see text in Section 3.1).

log from Ilbert et al. (2009) including the new UltraVISTA data from the DR1 (McCracken et al. 2012). Therefore, the offsets in Table 4 are slightly different from those in Table 1 of Ilbert et al. (2009).

Note that the magnitudes in the public catalog are not corrected for the Galactic extinction. Instead, we provide the Galactic extinction value, $E(B-V)$, from Schlegel et al. (1998) for each object in the catalog. The correction for the Galactic extinction in each band can be calculated from these values.

3.3 Data Quality

We estimated the limiting magnitudes using the 81 tiles (the COSMOS *HST*/ACS field) for each band. For each tile, we set 50,000 random points and performed aperture photometry with a $3''$ diameter aperture on the PSF-matched images which were convolved to the resolution of the COSMOS $K_{\rm s}$-band image. In order to measure the background fluctuation properly, we masked objects on the images. We used SExtractor version 2.3.2 (Bertin & Arnouts 1996) with the detection criteria of 5-pix connection above the 2σ significance. Then we replaced the masked regions with pseudo noise images, which were provided from randomly-shifted object-masked images. Then we evaluated the limiting magnitudes from the standard deviation for the distribution of the random photometry.

The average limiting magnitudes of the 81 tiles for the IA and NB711 bands are listed in Table 4. As shown in Table 4 and Figures 5 and 6, the 3σ limiting magnitudes are ~ 25.1–25.9 mag in IA427–IA827 bands. The NB711 data reach to the limiting magnitude of ~ 25.0 mag as shown in Table 4 and Figure 7. The standard deviation of the limiting magnitudes among the 81 tiles for each band is ~ 0.10–0.16 mag. As seen in Figures 5–7, the limiting magnitudes are brighter in the tiles at the edge of our survey field, because the total exposure time is smaller in these regions. Some tiles where very bright stars illuminate surrounding sky region also show brighter limiting magnitudes.

4 DISCUSSION

We present deep optical imaging observations made with the Suprime-Cam on the Subaru Telescope with 20 filters [6 broad-band, 12 intermediate-band (IA), and 2 narrow-band (NB) filters]: Subaru COSMOS 20. In this paper, we describe the details of our imaging with the 12 IA filters and NB711. Note that those of the other seven filters are given in Paper I.

The use of intermediate-band filters has generally a couple of scientific merits: (1) improvement of the accuracy of photometric redshifts and (2) selection of very strong emitters. First, we discuss the improvement of the accuracy of photometric redshifts. As described in Mobasher et al. (2007), our previous accuracy of photometric redshifts based on six Subaru broad band, CFHT u band, ACS F814W, NB816, and

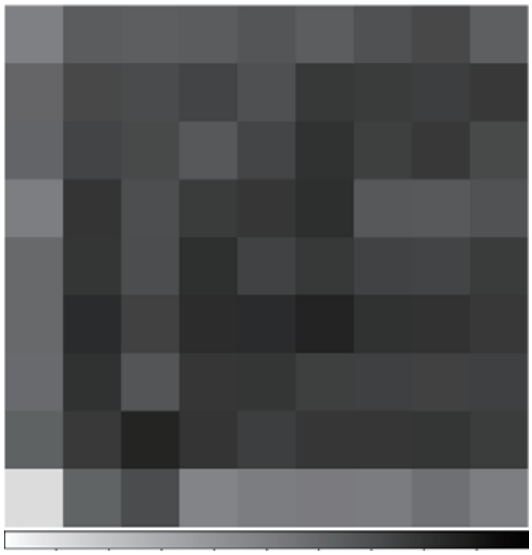

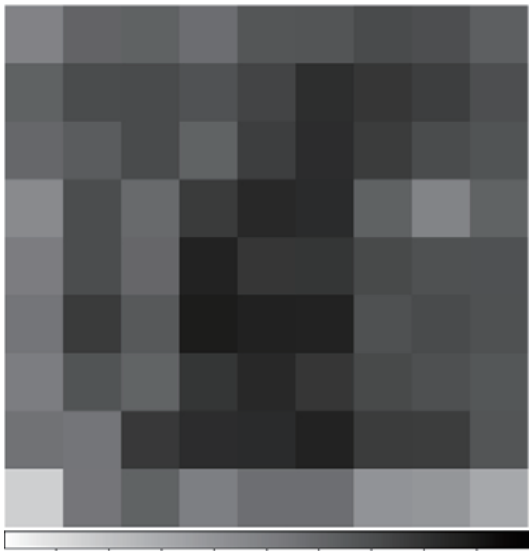

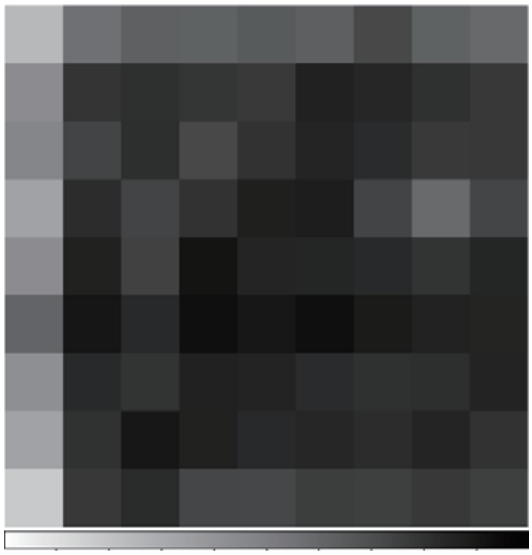

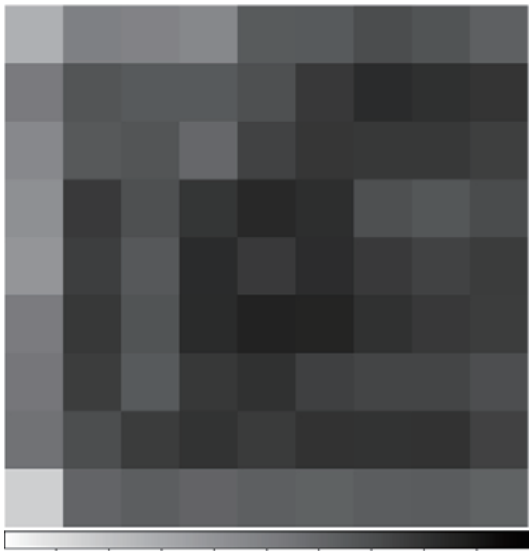

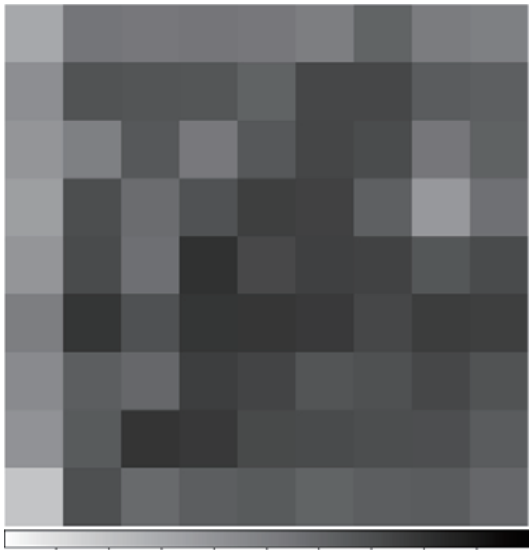

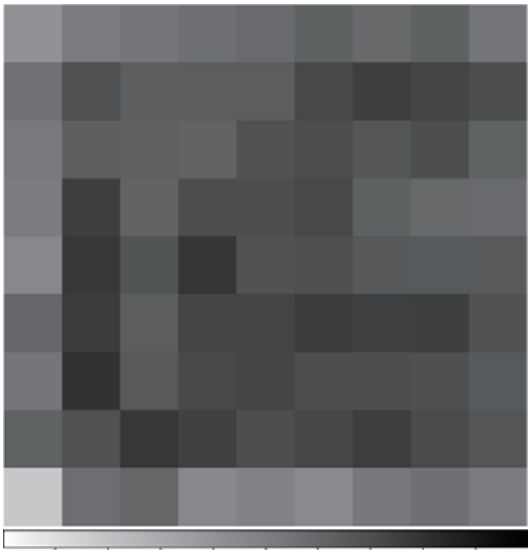

Fig. 5. Variations of 3σ limiting magnitudes within $3''$ diameter aperture in the 81 tiles of the $IA427$–, $IA464$–, $IA484$–, $IA505$–, $IA527$–, and $IA574$–band data from top-left to bottom-right.

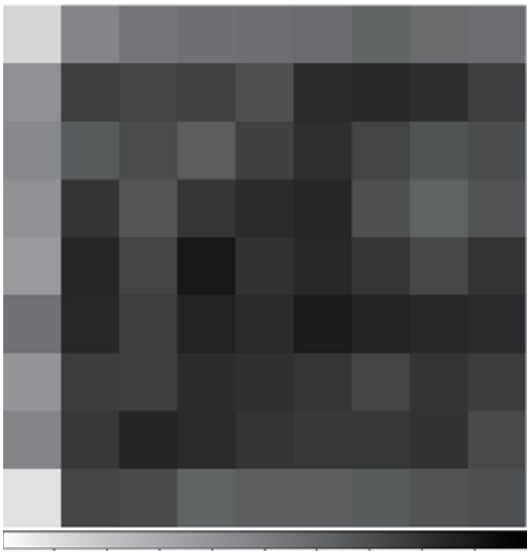

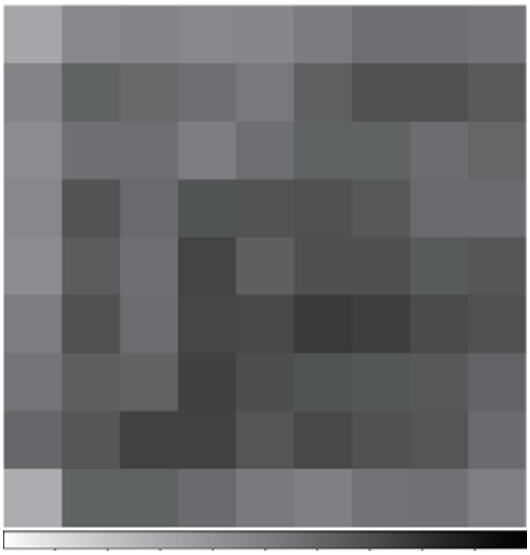

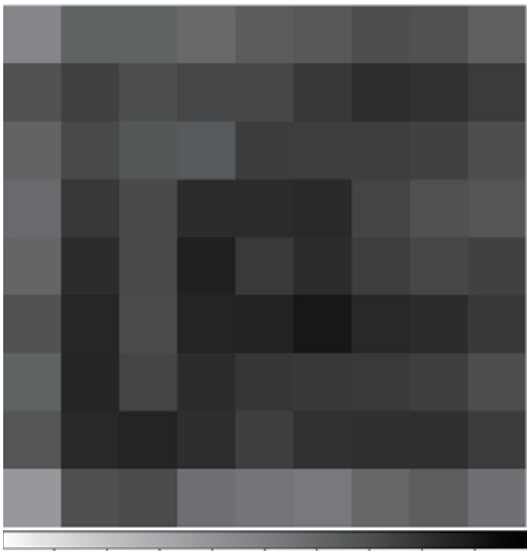

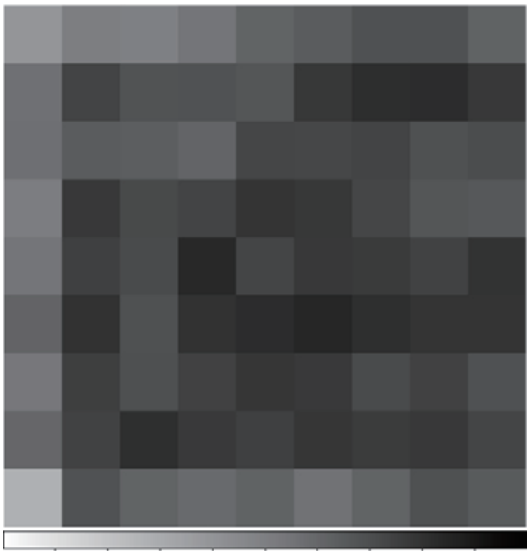

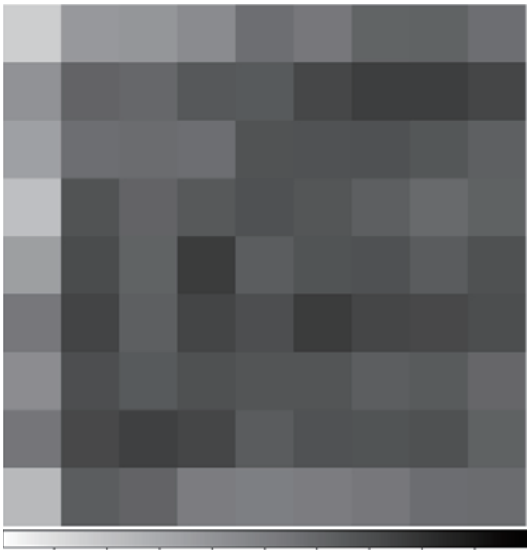

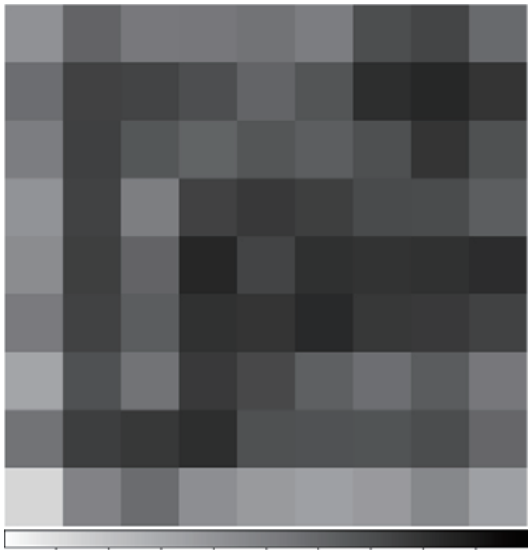

Fig. 6. Same as Figure 5, but for $IA624$–, $IA679$–, $IA709$–, $IA738$–, $IA767$–, and $IA827$–band data from top-left to bottom-right.

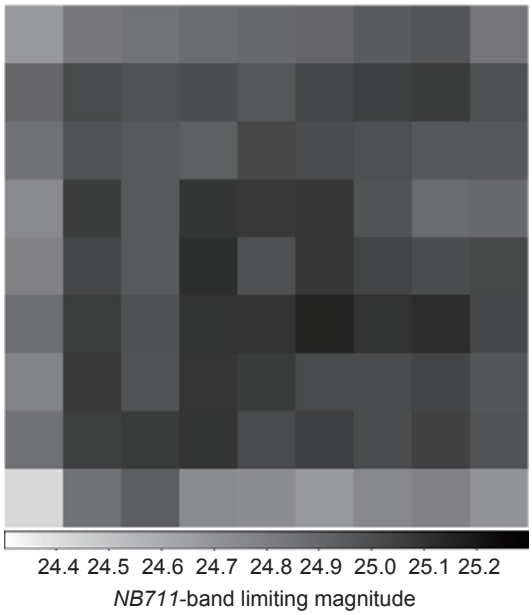

Fig. 7. Same as Figure 5, but for $NB711$–band data.

CTIO/KPNO $K_{\rm s}$ photometric data is $\sigma_{\Delta z} = 0.031$ where $\Delta z = (z_{\rm phot} - z_{\rm spec})/(1 + z_{\rm spec})$; note that $z_{\rm phot}$ and $z_{\rm spec}$ are photometric and spectroscopic redshifts, respectively. Since both u and $K_{\rm s}$ are used together with optical data, the accuracy of $z_{\rm phot}$ is better than that of typical optical studies (e.g., Hogg et al. 1998). However, in the COSMOS project, thanks to its multi-wavelength campaign, 30 band photometric data including Subaru COSMOS 20 data are accumulated to obtain much more accurate estimates of $z_{\rm phot}$ (Ilbert et al. 2009; see also Salvato et al. 2009, 2011). The accuracy of $z_{\rm phot}$ is improved to $\sigma_{\Delta z} = 0.007$ for $i < 22.5$. Even at fainter magnitudes of $i < 24$, the accuracy is found to be still high as $\sigma_{\Delta z} = 0.012$ for the galaxies at $z_{\rm spec} < 1.25$ (Ilbert et al. 2009).

There are several similar surveys with the use of intermediate band filters.

[1] COMBO-17 (Classifying Objects by Medium-Band Observations in 17 Filters): This is a pioneering optical survey with multi-band filters (Wolf et al. 2003). The COMBO-17 covers three $30' \times 30'$ fields, including the Extended Chandra Deep Field South (ECDF-S). In this survey, twelve intermediate-band filters were used together with five broad-band ones (U, B, V, R, and I) by using the Wide Field Imager at the MPG/ESO 2.2 m telescope on La Silla, Chile. Their intermediate-band filters cover 410 nm to 920 nm. The spectral resolution is not fixed for all the filters but ranges from $R = \lambda/\Delta\lambda = 14$ to 61 (mostly from 30 to 40). The use of intermediate-band filters improves the accuracy of photometric redshifts to $\sigma_{\Delta z} = 0.007$ for $R < 24$ (Wolf et al. 2004). This enables them to construct a large sample of AGNs at $z \sim$ 1–5.

[2] MUSYC (the Multiwavelength Survey by Yale-Chile): In this project, 18 intermediate-band filters in the IA filter system for Suprime-Cam on the Subaru Telescope were used together with 14 board-band data from optical to mid-infrared (seven optical filters from U to z, three near-infrared filters, J, H, and K, and four Spitzer IRAC bands, 3.6, 4.5, 5.8, and 8.0 μm) (Cardamone et al. 2010). These data cover a $30' \times 30'$ field of the ECDF-S, which is one of the MUSYC fields. The use of IA filters improves the accuracy of photometric redshifts at $z = 0.1$ to 1.2 and $z \geq 3.7$: $\sigma_{\Delta z} = 0.01$ for $R < 25$, see Table 8 in Cardamone et al. (2010) in more detail. This is attributed that the Balmer break (3648 Å) or Lyman break (912 Å) falls in wavelength interval covered by the 18 IA filters. According to Cardamone et al. (2010), *the use of IA filters not only tightens the accuracy of photometric redshifts but also can help to rule out false redshift solution (so called catastrophic failures)*.

[3] MAHOROBA-11: This survey is a scaled down version of Subaru COSMOS 20 (Yamada et al. 2005). In this survey seven IA filters are used together with five broad-band filters. These data cover a $34' \times 27'$ area in the Subaru XMM-Newton Deep Survey field. Their main purpose is to search for Lyα emitters at $z > 3.7$ by using a photometric redshift method. They showed that the fraction of false detection is only 10%.

[4] ALHAMBRA (the Advanced Large Homogeneous Area Medium-Band Redshift Astronomilca): This survey has been carried out by using the wide-field optical camera, Large Area Imager for Calar Alto (LAICA) on the Calar Alto 3.5 m telescope with 20 intermediate-band filters with 300 Å spacing (Moles et al. 2008; Molino et al. 2014). The surveyed area size is 2.79 deg^2. The accuracy of photometric redshifts is $\sigma_{\Delta z} = 0.01$ for $I < 22.5$ and $\sigma_{\Delta z} = 0.014$ for $22.5 < I < 24.5$.

In this way, a number of optical wide-field deep surveys have been carried out by using their original intermediate-band filter systems. The main reason for this is to obtain more reliable photometric redshifts for large numbers of objects in the individual surveys; see Figure 1B in Molino et al. (2014) for a comprehensive comparison among available optical surveys including surveys with broad-band filters only such as HDF, SDSS, and so on. The Subaru COSMOS 20 is the widest survey among the deep ($m_{\rm lim} \sim 25$) optical intermediate-band surveys. Some efficient multiple-object spectrographs are available on 8 m class telescopes (e.g., VIMOS on the VLTs and FMOS on the Subaru Telescope). However, imaging surveys with intermediate-band filters are more efficient to obtain redshift information for large numbers of objects.

We mention about our future works on study of strong emission-line objects. The wide imaging with the IA filter set of the Subaru COSMOS 20 enables us to detect very strong emission-line objects (star forming galaxies and AGNs) over a extremely large volume. In our forthcoming papers, we will present a large sample of IA-excess strong emission-line objects (Kajisawa et al. 2015, in preparation) and a new population of

MAESTLO (= MAssive Extremely STrong Lyα Emitters) at $z \sim 3$ with rest-frame Lyα equivalent width of $\mathrm{EW}_0(\mathrm{Ly}\alpha) \geq 100$ Å and $M_{\rm star} \geq 10^{10.5}\ M_\odot$ (Taniguchi et al. 2015).

Finally, we note that the major COSMOS datasets including the Subaru images and catalogs are publicly available (following calibration and validation) through the web site for IPAC/IRSA:
http://irsa.ipac.caltech.edu/data/COSMOS/.

ACKNOWLEDGMENTS

The *HST* COSMOS Treasury program was supported through NASA grant HST-GO-09822. We gratefully acknowledge the contributions of the entire COSMOS collaboration consisting of more than 70 scientists. More information on the COSMOS survey is available at **http://www.astro.caltech.edu/~cosmos**. It is a pleasure the acknowledge the excellent services provided by the NASA IPAC/IRSA staff (Anastasia Laity, Anastasia Alexov, Bruce Berriman and John Good) in providing online archive and server capabilities for the COSMOS datasets. We are deeply grateful to the referee for his/her useful comments and excellent refereeing, which helped us to improve this paper very much. We would also like to thank the staff at the Subaru Telescope for their invaluable help. In particular, we would like to thank Hisanori Furusawa because his professional help as a support scientist made our Suprime-Cam observations successful. Data analysis were in part carried out on common use data analysis computer system at the Astronomy Data Center, ADC, of the National Astronomical Observatory of Japan. This work was financially supported in part by JSPS (YT: 15340059, 17253001, 19340046, 23244031, TN: 23654068 and 25707010) and by the Yamada Science Foundation (TN).

References

Ajiki, M., Taniguchi, Y., Fujita, S. S., et al. 2004, PASJ, 56, 597
Amorín, R., Grazian, A., Castellano, M., et al. 2014, ApJL, 788, L4
Amorín, R., Pérez-Montero, E., Contini, T., et al. 2015, A&A, 578, A105
Atek, H., Siana, B.,Scarlata, C., et al. 2011, ApJ, 743, 121
Bertin, E., & Arnouts, S. 1996, A&AS, 117, 393
Bohlin, R. C. 1996, AJ, 111, 1743
Bohlin, R. C., Dickinson, M. E., & Calzetti, D. 2001, AJ, 122, 2118
Capak, P., Aussel, H., Ajiki, M., et al. 2007, ApJS, 172, 99
Cardamone, C., Schawinski, K., Sarzi, M., et al. 2009, MNRAS, 399, 1191
Cardamone, C. N., van Dokkum, P. G., Urry, C. M., et al. 2010, ApJS, 189, 270
Elvis, M., Civano, F., Vignali, C., et al. 2009, ApJS, 184, 158
Feruglio, C., Aussel, H., Le Floc'h, E., et al. 2010, ApJ, 721, 607
Fujita, S. S., Ajiki, M., Shioya, Y., et al. 2003, AJ, 125, 13
Georgakakis, A., Mountrichas, G., Salvato, M., et al. 2014, MNRAS, 443, 3327
Hasinger, G., Cappelluti, N., Brunner, H., et al. 2007, ApJS, 172, 29
Hayashino, T., Tamura, H., Matsuda, Y., et al. 2003, Publications of the National Astronomical Observatory of Japan, 7, 33
Hayashino, T., Taniguchi, Y., Yamada, T., et al. 2000, Proc. SPIE, 4008, 397
Hogg, D. W., Cohen, J. G., Blandford, R., et al. 1998, AJ, 115, 1418
Hopkins, A. M. 2004, ApJ, 615, 209
Hu, E. M., Cowie, L. L., Barger, A. J., et al. 2010, ApJ, 725, 394
Hu, E. M., Cowie, L. L., Capak, P., et al. 2004, AJ, 127, 563
Ideue, Y., Nagao, T., Taniguchi, Y., et al. 2009, ApJ, 700, 971
Ideue, Y., Taniguchi, Y., Nagao, T., et al. 2012, ApJ, 747, 42
Iye, M., Karoji, H., Ando, H., et al. 2004, PASJ, 56, 381
Ilbert, O., Arnouts, S., McCracken, H. J., et al. 2006, A&A, 457, 841
Ilbert, O., Capak, P., Salvato, M., et al. 2009, ApJ, 690, 1236
Kaifu, N., Usuda, T., Hayashi, S. S., et al. 2000, PASJ, 52, 1
Kajisawa, M., Shioya, Y., Aida, Y., et al. 2013, ApJ, 768, 51
Kakazu, Y., Cowie, L. L., & Hu, E. M. 2007, ApJ, 668, 853
Kashikawa, N., Shimasaku, K., Yasuda, N., et al. 2004, PASJ, 56, 1011
Kobayashi, M. A. R., Murata, K. L., Koekemoer, A. M., et al. 2015, submitted to ApJ
Kodaira, K., Taniguchi, Y., Kashikawa, N., et al. 2003, PASJ, 55, L17
Koekemoer, A. M., Aussel, H., Calzetti, D., et al. 2007, ApJS, 172, 196
Kovač, K., Lilly, S. J., Knobel, C., et al. 2014, MNRAS, 438, 717
McCracken, H. J., Milvang-Jensen, B., Dunlop, J., et al. 2012, A&A, 544, A156
Miyazaki, S., Komiyama, Y., Nakaya, H., et al. 2012, Proc. SPIE, 8446,
Miyazaki, S., Komiyama, Y., Sekiguchi, M., et al. 2002, PASJ, 54, 833
Mobasher, B., Capak, P., Scoville, N. Z., et al. 2007, ApJS, 172, 117
Moles, M., Benítez, N., Aguerri, J. A. L., et al. 2008, AJ, 136, 1325
Molino, A., Benítez, N., Moles, M., et al. 2014, MNRAS, 441, 2891
Monet, D. G., Levine, S. E., Canzian, B., et al. 2003, AJ, 125, 984
Murata, K. L., Kajisawa, M., Taniguchi, Y., et al. 2014, ApJ, 786, 15
Murayama, T., Taniguchi, Y., Scoville, N. Z., et al. 2007, ApJS, 172, 523
Nagao, T., Murayama, T., Maiolino, R., et al. 2007, A&A, 468, 877
Nagao, T., Sasaki, S. S., Maiolino, R., et al. 2008, ApJ, 680, 100
Radovich, M., Bonnarel, F., Mellier, Y., et al. 2001, The New Era of Wide Field Astronomy, 232, 297
Salvato, M., Hasinger, G., Ilbert, O., et al. 2009, ApJ, 690, 1250
Salvato, M., Ilbert, O., Hasinger, G., et al. 2011, ApJ, 742, 61
Sanders, D. B., Salvato, M., Aussel, H., et al. 2007, ApJS, 172, 86
Schinnerer, E., Carilli, C. L., Scoville, N. Z., et al. 2004, AJ, 128, 1974
Schinnerer, E., Smolčić, V., Carilli, C. L., et al. 2007, ApJS, 172, 46
Schlegel, D. J., Finkbeiner, D. P., & Davis, M. 1998, ApJ, 500, 525
Scoville, N., Abraham, R. G., Aussel, H., et al. 2007a, ApJS, 172, 38
Scoville, N., Arnouts, S., Aussel, H., et al. 2013, ApJS, 206, 3
Scoville, N., Aussel, H., Brusa, M., et al. 2007b, ApJS, 172, 1
Shimasaku, K., Ouchi, M., Furusawa, H., et al. 2005, PASJ, 57, 447
Shioya, Y., Taniguchi, Y., Ajiki, M., et al. 2005, PASJ, 57, 287
Shioya, Y., Taniguchi, Y., Sasaki, S. S., et al. 2008, ApJS, 175, 128
Shioya, Y., Taniguchi, Y., Sasaki, S. S., et al. 2009, ApJ, 696, 546
Smolčić, V., Aravena, M., Navarrete, F., et al. 2012, A&A, 548, A4
Takahashi, M. I., Shioya, Y., Taniguchi, Y., et al. 2007, ApJS, 172, 456
Taniguchi, Y. 2004, Studies of Galaxies in the Young Universe with New Generation Telescope, Proceedings of Japan-German Seminar, held in Sendai, Japan, July 24-28, 2001, Eds.: N. Arimoto and W. Duschl, 2004, p. 107-111
Taniguchi, Y., Ajiki, M., Nagao, T., et al. 2005, PASJ, 57, 165
Taniguchi, Y., Kajisawa, M., Kobayashi, M. A. R., et al. 2015, ApJL, 809, L7

Table A1. A summary of IA filters.

Band	λ_c^a (Å)	FWHM^b (Å)
$IA427$	4271	210
$IA445$	4456	203
$IA464$	4636	217
$IA484$	4842	227
$IA505$	5063	232
$IA527$	5272	242
$IA550$	5512	273
$IA574$	5743	271
$IA598$	6000	294
$IA624$	6226	299
$IA651$	6502	322
$IA679$	6788	336
$IA709$	7082	318
$IA738$	7371	322
$IA767$	7690	364
$IA797$	7981	353
$IA827$	8275	340
$IA856$	8566	325
$IA907$	9068	423
$IA965$	9651	469

[a] Center wavelength defined as the center of the two wavelengths at which the filter transmission becomes the half maximum.
[b] FWHM calculated from the same filter response curve used to evaluate the center wavelength.

Taniguchi, Y., Murayama, T., Scoville, N. Z., et al. 2009, ApJ, 701, 915
Taniguchi, Y., Scoville, N., Murayama, T., et al. 2007, ApJS, 172, 9 (Paper I)
Taniguchi, Y., Shioya, Y., & Trump, J. R. 2010, ApJ, 724, 1480
Wolf, C., Meisenheimer, K., Kleinheinrich, M., et al. 2004, A&A, 421, 913
Wolf, C., Wisotzki, L., Borch, A., et al. 2003, A&A, 408, 499
Yamada, S. F., Sasaki, S. S., Sumiya, R., et al. 2005, PASJ, 57, 881
Zamojski, M. A., Schiminovich, D., Rich, R. M., et al. 2007, ApJS, 172, 468

Appendix A Intermediate-band filter system for Suprime-Cam

In this section, we present optical properties of the IA filter system for Suprime-Cam on the Subaru Telescope. This filter system was developed as a private type of filters by the two authors (TH and YT). Early short descriptions on this filter system are given in Hayashino et al. (2000) and Taniguchi (2004).

The IA filter system consists of 20 intermediate band filters with a spectral resolution of $R = 20$–26, covering 410 nm to 1000 nm. (Table A1). The filter response curves are shown in Figure A1. Note that these response curves are those of the filters themselves; that is, the effects of the CCD sensitivity, the atmospheric transmission, and the transmission of the telescope and the instrument are not included.

Table A2. The Specifications for the Subaru IA Filter System.

Item	Specification	
Clear aperture	$185\ \mathrm{mm} \times 150\ \mathrm{mm}$	
Peak transmittance (T_{peak})	$> 70\%$ ($> 80\%$ goal)	
Homogeneity of T_{peak}	$< 5\%$	
Ripple (valley/peak)	$> 85\%$	
Linear change (valley/peak)	$> 90\%$	
λ_{eff} tolerance	$< \pm 0.25\%$ of λ_{eff}	
FWHM tolerance	$< \pm 0.25\%$ of λ_{eff}	
Bubble	$d < 0.1\ \mathrm{mm}$	acceptable
	$d = 0.1$–$0.2\ \mathrm{mm}$	≤ 5 bubbles
	$d = 0.2$–$0.5\ \mathrm{mm}$	≤ 3 bubbles
	$d > 0.5\ \mathrm{mm}$	Not allowed
Stain	Not allowed	

All the IA filters were manufactured by Barr Associates Co. Ltd (now, Materion Co. Ltd). The specifications for the IA filters are summarized in Table A2. Although some of the specifications were found not to be fully satisfied, all the filters are highly useful for scientific observations (e.g., Fujita et al. 2003; Ajiki et al. 2004; Shioya et al. 2005; Yamada et al. 2005; Nagao et al. 2008). Details of measurements of the filter transmission is given in Hayashino et al. (2003). The measured data are available at http://www.awa.tohoku.ac.jp/astro/filter.html.

Appendix B IA-band magnitudes of the standard stars

In Table B1, we summarize the theoretical IA-band magnitudes of the standard stars computed from the CALSPEC spectra and the complete system response, in AB magnitudes. The uncertainty given here assumes a perfect knowledge of the system response and are based solely on the CALSPEC statistical and systematic uncertainties.

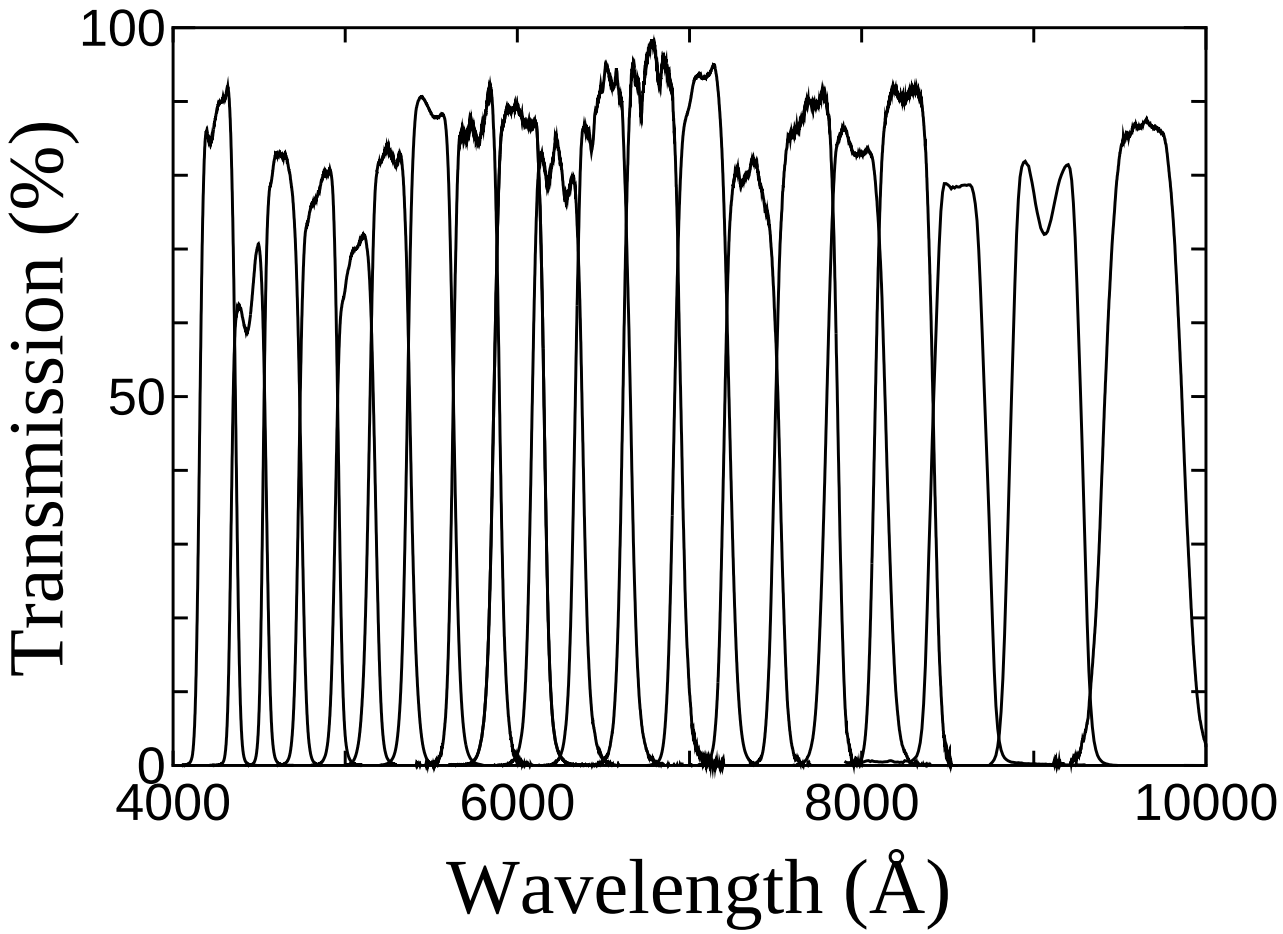

Fig. A1. The filter response curves themselves measured at the center of the 20 intermediate-band filters. Note that these curves do not include the effects of the CCD sensitivity, the atmospheric transmission, and the transmission of the telescope and the instrument.

Table B1. Theoretical IA-band magnitudes of the standard stars.

Band	GD 50	GD 108	HZ 4	HZ 21	HZ 44
$IA427$	13.690 ± 0.002	13.187 ± 0.002	14.445 ± 0.002	14.191 ± 0.002	11.223 ± 0.001
$IA464$	13.749 ± 0.002	13.297 ± 0.002	14.252 ± 0.002	14.405 ± 0.002	11.374 ± 0.002
$IA484$	13.869 ± 0.003	13.414 ± 0.003	14.576 ± 0.004	14.474 ± 0.003	11.447 ± 0.002
$IA505$	13.893 ± 0.003	13.442 ± 0.003	14.385 ± 0.026	14.528 ± 0.026	11.516 ± 0.025
$IA527$	13.975 ± 0.003	13.504 ± 0.003	14.394 ± 0.046	14.605 ± 0.047	11.583 ± 0.045
$IA574$	14.164 ± 0.003	13.650 ± 0.003	14.534 ± 0.001	14.771 ± 0.001	11.747 ± 0.001
$IA624$	14.309 ± 0.002	13.774 ± 0.002	14.662 ± 0.001	14.919 ± 0.001	11.896 ± 0.001
$IA679$	14.485 ± 0.003	13.917 ± 0.003	14.833 ± 0.001	15.097 ± 0.001	12.073 ± 0.001
$IA709$	14.559 ± 0.003	13.984 ± 0.003	14.849 ± 0.001	15.176 ± 0.001	12.154 ± 0.001
$IA738$	14.634 ± 0.002	14.052 ± 0.002	14.912 ± 0.001	15.251 ± 0.001	12.231 ± 0.001
$IA767$	14.698 ± 0.003	14.119 ± 0.003	14.980 ± 0.001	15.339 ± 0.001	12.321 ± 0.001
$IA827$	14.844 ± 0.002	14.237 ± 0.002	15.093 ± 0.002	15.491 ± 0.002	12.468 ± 0.001
$NB711$	14.566 ± 0.004	13.992 ± 0.004	14.860 ± 0.002	15.194 ± 0.003	12.167 ± 0.002